AFCRL-65-707
SEPTEMBER 1965
INSTRUMENTATION PAPERS, NO. 81

AIR FORCE CAMBRIDGE RESEARCH LABORATORIES
L. G. HANSCOM FIELD, BEDFORD, MASSACHUSETTS

Pressure Gradients in Bridgman Anvil Devices

L. C. TOWLE
R. E. RIECKER

Sponsored by
Advanced Research Projects Agency
Vela Uniform
ARPA Order No. 292

OFFICE OF AEROSPACE RESEARCH
United States Air Force

AFCRL-65-707
SEPTEMBER 1965
INSTRUMENTATION PAPERS, NO. 81

TERRESTRIAL SCIENCES LABORATORY PROJECT 7639

AIR FORCE CAMBRIDGE RESEARCH LABORATORIES

L. G. HANSCOM FIELD, BEDFORD, MASSACHUSETTS

Pressure Gradients in Bridgman Anvil Devices

L. C. TOWLE*

R. E. RIECKER

*Allis Chalmers Man. Co., Milwaukee 1, Wisconsin

Sponsored by
Advanced Research Projects Agency
Vela Uniform
ARPA Order No. 292

OFFICE OF AEROSPACE RESEARCH
United States Air Force

Abstract

Experimental evidence regarding pressure gradients in Bridgman anvil devices is reviewed and some new experimental data are presented. Although there are many differences in details, all the experimental evidence is found to fit a general pattern. A simple empirical relationship describing the pressure distribution is derived which is consistent with experimental observation. The experimentally determined pressure is used to estimate errors introduced into various types of anvil experiments by pressure gradients. Numerical values for the correction factors are given in graphical form for a wide range of experimental conditions. Analysis of shear experiments indicates that pressure gradients are much smaller under dynamic conditions. Analysis also shows that the peripheral sample region which is partially non-load-supporting frequently has a greater detrimental effect on anvil experiments than does the pressure gradient which exists over the central portion of the sample cell.

BLANK PAGE

Contents

1. INTRODUCTION 1

2. EXPERIMENTAL OBSERVATIONS 5

3. EMPIRICAL ANALYSIS 7

   3.1 Static Anvil Experiments 13
   3.2 Dynamic Anvil Experiments 15

4. CONCLUSIONS 24

ACKNOWLEDGMENTS 27

REFERENCES 27

Illustrations

1. A Normalized Plot of the Experimental Pressures at which Known Phase Transitions Were Observed to Occur as a Function of the Radial Position of the Calibrant Wire 6

2. The Sample Pressure as a Function of Radial Position as Calculated from an Empirical Equation Derived in the Text 9

3. A Typical Plot of Turning Moment versus Nominal Applied Pressure as Observed in Shearing Experiments. The knee in the curve separates the low pressure realm in which surficial slippage occurs from the high pressure realm in which internal shearing of the sample occurs 17

4. The Correction Factor $Q(\alpha, \rho_e)$ as a Function of the Parameters α and ρ_e. This factor is defined in the text, Eq. (20) 19

5. The ratio $R(\alpha, \rho_e)$ as a Function of the Parameters α and ρ_e. This factor is defined in the text, Eq. (26) 21

6. The Correction Factor $T(\alpha, \rho_e, \mu Z)$ as a Function of the Parameters α and ρ_e for the Special Case $\mu Z = 2.0$. These factors are defined in the text, Eqs. (33) and (34) 24

Pressure Gradients in Bridgman Anvil Devices

I. INTRODUCTION

Opposed anvils are the simplest and most widely used form of very-high-pressure apparatus. Bridgman (1935, 1936, 1937) used them extensively in the vicinity of room temperature and they are now being used at high and low temperatures as well. They have been used to investigate a wide range of physical phenomena. Although it has long been realized that truly hydrostatic pressures were not obtained with anvils, the magnitude of the pressure gradients which can exist in this type of apparatus was not appreciated fully until recently. The nature of the possible pressure gradients and their influence on certain types of measurements constitute the subject of this paper.

For purposes of discussion it is convenient to divide opposed anvil devices into categories - static and dynamic. Most opposed anvil devices are static, which means that the anvils are not rotated relative to each other. A relatively small number are dynamic, in which one anvil is rotated or oscillated while the other is held stationary. The dynamic type is used primarily for shear strength measurements or in phase equilibrium investigations.

The pressure distribution in a sample compressed between anvils may depend significantly on whether the anvils are static or dynamic. It will also depend on

(Received for publication 10 August 1965)

the nature of the sample, the anvil material, the temperature and pressure applied, the geometrical arrangement, and other factors. In a dynamic device the pressure distribution may depend on the rate of strain of the sample material.

The composition and structure of the wafer-like sample cell used in an anvil apparatus vary markedly from one experiment to the next. In shear strength measurements and some geochemical investigations the sample cell consists of a homogeneous disc, but this simple configuration is the exception rather than the rule. Most experimental arrangements consist of a central disc surrounded by an annular ring which retains the sample between the anvils. Pyrophyllite is commonly used for the retaining ring, although stainless steel or nickel are sometimes employed. The properties and dimensions of the retaining ring relative to those of the central disc have an important bearing on the pressure distribution.

The central disc in the sample cell may be the material under investigation or it may serve only as a pressure transmitting medium. In the latter case the sample itself may be a wire or foil on which electrical or other measurements are to be made. The presence of such a specimen embedded in the central disc further complicates the pressure distribution. This marked variation in the composition of the sample cell greatly complicates the problem of determining the pressure gradient between opposed anvils, and no doubt is partly responsible for the widely different gradients reported.

Bridgman (1937) calculated the deformation of anvils under pressure using classical elasticity theory assuming a uniform pressure distribution.

His analysis predicted that the anvils and sample wafer would assume a lenticular shape when compressed. Because the permanent deformation of anvils and sample wafers conformed to his prediction, he assumed that a uniform pressure distribution was a satisfactory first approximation. Bridgman also believed that a more careful analysis would show that the maximum pressures occurred in an annular region concentric with the axis of compression. Recent experimental work has shown this qualitative description to be valid in some instances but not in others.

Christiansen et al (1962) determined the pressure distribution between anvils using silica glass as a pressure indicator. They established that, on compression at room temperature, this material experiences a permanent densification which is linearly related to the pressure. In compression tests on 0.24-in.-diam glass wafers, the pressure near the edge of the disc was much larger than at the center, 100 kilobars vs 70 kilobars in a typical case when the nominal applied pressure was about 73 kilobars. In another series of tests, in which the glass disc was encircled by a pipestone retaining ring, the average pressure on the glass disc was greater than the nominal applied pressure by from 10 to 25 percent. Unfortunately the pressure gradient was not determined in the latter experiments.

Although these results may be considered typical because they demonstrate the occurrence of substantial pressure gradients and also tend to confirm Bridgman's qualitative description, they are unusual. In most experimental configurations, the maximum pressure occurs at the center of the anvils. Pressure multiplication effects have been reported in which the pressure at the center is as much as 2 or 2.5 times the nominal applied pressure.

For example, Myers et al (1963) made a rather extensive investigation on a sample wafer design consisting of a pyrophyllite disc surrounded by a nickel retaining ring. Small calibrant wires were located at various radial positions. The wires were fabricated from materials having known phase transitions which can be detected electrically. Thus the nominal applied pressure required to produce a known transition pressure could be measured as a function of the radial position of the calibrant wire. The measurements did not determine the pressure gradient directly; however they did demonstrate that substantial pressure gradients must exist. In particular it was found that the pressure at the center of the anvils might be either greater or less than the nominal applied pressure, depending on the diameter-to-thickness ratio of the sample wafer. For thick samples a pressure multiplication of as much as 2.5 was observed at the center of the anvils while for thin samples a pressure deficiency was noted. The multiplication effect was observed over a wide range of pressures, and the ratio of nominal applied pressure to actual pressure at the center of the anvils was practically constant in the range up to 90 kilobars.

Montgomery et al (1963) have investigated the pressure gradient in a silver chloride disc surrounded by a pyrophyllite retaining ring. They report a dependence of the central pressure on the diameter-to-thickness ratio which is qualitatively the same as that found by Myers et al. Using calibrant wires located at various radial positions they also demonstrated that a large pressure gradient existed in the silver chloride discs. The nominal applied pressure required to produce the bismuth I-II transition was related linearly to the radial position of the calibrant wire. Similar observations developed using the bismuth VI-VIII transition. The fit to the straight line is very good, the experimental reproducibility being a few percent. It is important to note that this does not necessarily imply a linear pressure gradient for reasons which will be discussed.

Montgomery et al also showed that manganin wires in the form of circular arcs concentric with the center of the anvils gave very reproducible plots of relative resistance vs nominal applied pressure. Hysteresis observed remained within the uncertainty of the measurements, and wires of different radii and arc length yielded resistance plots of similar shape. Since manganin is very strain-sensitive, these results showed clearly that the pressure distribution had the axial symmetry expected.

It was also discovered, by making a single plausible assumption that the pressure at any radial position was always proportional to the nominal applied pressure, that all relative resistance data obtained with wires of different radii could be superimposed to form a single curve of relative resistance versus pressure. The assumption was confirmed for the center of the anvils by Myers et al, as noted previously. The calibration curve was used to calculate the pressure distribution between the anvils at several pressures and it was found that the central pressure was less than the nominal applied pressure and that the pressure increased linearly with radial position.

In order to make the calculations, an additional plausible assumption was made, that the pressure dropped abruptly in a linear manner to some small value comparable to the shear strength of the retaining ring in the region near the periphery of the sample. The width of this region was about 0.030 in. This on 1/2-in.-diam anvils an annular ring comprising about 23 percent of the total anvil area supported only a small fraction of the applied load. Also, the size of this transition region was independent of the anvil size and the applied load.

The existence of this border region is also evident from a series of compression tests on homogeneous wafers of several materials made by Vaisnys and Montgomery (1964). They discovered that the load-bearing area of the anvils varied from 100 percent to 50 percent of the geometrical area, depending on the material compressed and on the diameter-to-thickness ratio. Thick samples resulted in the smallest load-bearing areas in agreement with the pressure-multiplication effect observed by others.

The pressure distribution between miniature diamond anvils has been observed optically by Duecker and Lippincott (ASME Paper, to be published) on homogeneous discs. A pressure multiplication effect of two or more was found at low pressures but the effect diminished at high pressures. However, the constant ratio of central pressure to nominal applied pressure observed by Myers et al in the high-pressure region, and assumed by Montgomery et al, was not observed. At low loads the radial pressure distribution appeared approximately parabolic and a theoretical model was given which correlated well with the observations. At nominal applied pressures of 20 kilobars or more, the observations fit a linear pressure distribution rather well with the exception of a small area at the center of the anvils. Since the pressures near the anvil edges were on the order of a kilobar, the observed pressure gradients were gigantic.

It remains difficult to draw any general conclusions from the fragmentary evidence available. The principal observations have been briefly summarized and it is clear that they are contradictory in some instances. Before an attempt is made to summarize the experimental evidence, Section 2 of this paper will describe some new observations relative to the pressure distribution. Section 4 is an attempt to assess the effect of the observed pressure gradients on various types of measurements.

2. EXPERIMENTAL OBSERVATIONS

A dynamic type of opposed anvil apparatus has been in use at AFCRL for several years. The design of the apparatus incorporates several novel features which have been described in the literature by Riecker (1964). The shear press is used in a comprehensive program of shear strength measurements on a variety of rock and mineral materials under geophysically realistic conditions of temperature and pressure (Riecker and Seifert, 1964a, 1964b).

A series of static compression tests were conducted on compressed mineral wafers approximately 0.020 in. thick and 1/4 in. or 1/2 in. in diameter. The wafers were compacted from the mineral olivine after it had been ground to pass a 400-mesh screen. The maximum and median grain sizes were 0.037 mm and 0.0043 mm, respectively.

Bismuth and thallium wires 0.010 in. in diameter and 0.014 in. long were placed vertically in the prepared wafers at various distances from the sample center. Thin platinum sheets were sandwiched above and below the mineral wafer to complete the electrical calibration cell. Resistance discontinuities indicate the bismuth I-II and thallium II-III phase transformations at 25.4 and 36.7 kilobars, respectively. The nominal applied pressure required to produce the known transitions in the calibrant wires was recorded as a function of the radial position of the wire. Observed pressures were divided by the appropriate transition pressure in order to form a dimensionless parameter. This parameter and its reciprocal are plotted in Figure 1 against the sample position with the latter expressed as a fraction of the anvil radius. It is evident that pressure gradients were present.

It should be noted that when expressed in this normalized fashion the data obtained on the bismuth and thallium fall on a single line. This implies that the pressure at a given radial position is proportional to the nominal applied pressure. A similar observation was made by Myers et al over a wider pressure range. The connection between Figure 1 and the actual pressure gradients will be developed in the next section, but first some qualitative observations need to be added.

In the static compression experiments the presence of large pressure gradients was also revealed by button-like central indentations produced in the anvils, similar to the effects described by Bridgman (1937). This manifestation of the pressure gradient has only been observed in static tests; in shear measurements this sort of permanent deformation of the anvils develops very rarely. No indentation occurs in static compression tests when the sample wafer thickness is less than 0.018 in. for 1/2-in.-diam anvils or 0.014 in. for 1/4-in.-diam anvils. This observation agrees qualitatively with that made by Myers et al; the pressure multiplication effect is greatest for sample geometries with small diameter-to-thickness ratios.

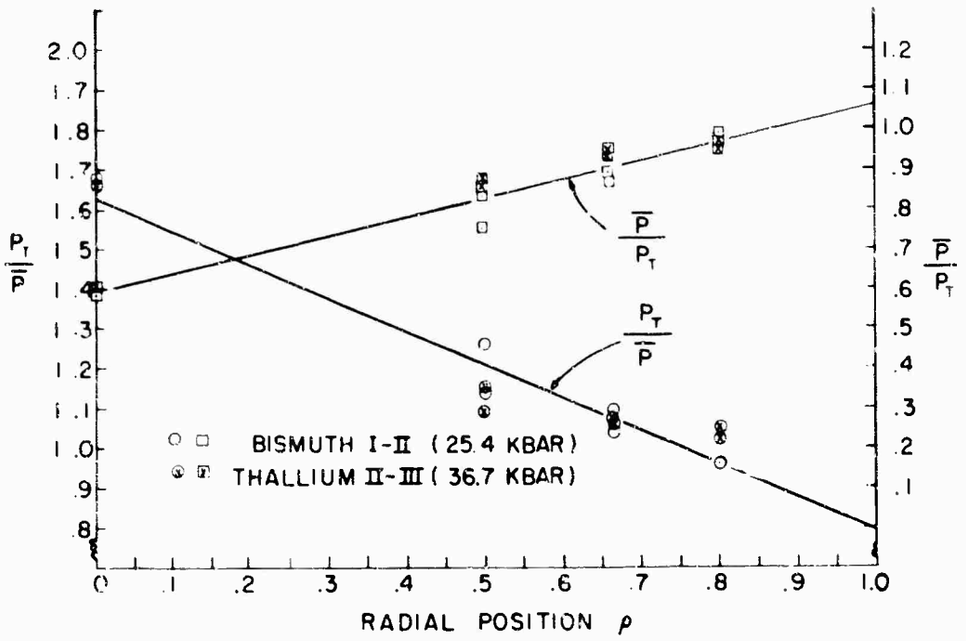

Figure 1. A Normalized Plot of the Experimental Pressures at which Known Phase Transitions Were Observed to Occur as a Function of the Radial Position of the Calibrant Wire

Qualitative observations made with the AFCRL apparatus suggest that under dynamic conditions the superimposed shear strain greatly reduces the pressure gradient which might otherwise be present in the sample. In addition, high temperature usually significantly reduces the gradient magnitude. For example, in static compression tests on enstatite, anvil deformation was observed at room temperature, but at temperatures of 300°C and above, significant deformation did not occur, even at pressures up to 75 kilobars. When test wafers are first heated at zero pressure, sheared also at zero pressure, and then raised to the test pressure, the pressure gradients appear to be minimal. This sequence permits the efficient extrusion of excess sample material early in the pressurization and allows a wafer to develop an equilibrium thickness of from six to eight mils. With this technique, any reasonable diameter-to-thickness ratio may be used with satisfactory results. Samples which initially ranged in thickness from 0.010 in. to 0.040 in. yielded equivalent shear strength or friction measurements within ±2 percent when sheared on either 1/4-in. or 1/2-in.-diam anvils. Unfortunately similar procedures cannot be used to eliminate the pressure gradients in static compression tests. In the static tests the actual sample configuration must be evaluated experimentally to ensure that pressure gradients are minimized.

On the basis of the limited evidence available, the following generalizations are made:

1. Using sample materials and geometries commonly employed, large pressure gradients may occur in static anvil devices.

2. The maximum pressure usually occurs at the center of the anvils and may be as much as 2.5 times the nominal applied pressure.

3. The magnitude of the pressure multiplication effect is markedly dependent on the sample geometry, and even a pressure deficiency at the anvil center may occur in thin sample wafers. In the latter case the maximum pressure will occur in an annular ring concentric with the axis of symmetry as predicted by Bridgman.

4. Frequently the pressure at a given radial position is proportional to the nominal applied pressure over a wide range of loads.

5. A transition region occurs around the periphery of a compressed sample wafer in which very large pressure gradients are to be expected because this region does not support its share of the applied load. The details of the pressure distribution in this region are completely unknown at present.

6. Direct evidence concerning the pressure gradients in dynamic anvils is practically nonexistent because of severe experimental difficulties. However indirect evidence cited previously suggests that pressure gradients occurring under dynamic conditions are much smaller than in static experiments.

5. EMPIRICAL ANALYSIS

Several theoretical attempts have been made to determine the pressure gradients existing in opposed anvils under static conditions (Jamieson and Lawson, 1962; Jackson and Waxman, 1962; Jackson and Davis, to be published). These have not yet proved to be of great value. The present writers approach the problem empirically, realizing that although the results will be less satisfying esthetically, the empirical approach may be better suited to their purpose.

The analysis proceeds in two steps. The first is to find an empirical expression representing the pressure distribution between compressed anvils which is simple enough to be analytically useful, and complex enough to be compatible with the experimental evidence. The second step is to perform calculations using the empirical equation for the pressure distribution in order to determine the magnitude of the errors introduced into various types of anvil experiments by the pressure gradients. Shear strength measurements are the primary concern and the aim is to determine the order of magnitude of the errors which can arise; for example, whether the computed shear strengths can be considered accurate to 5 or 50 percent. Thus certain assumptions which are obviously over-simplifications will be made in the interest of analytical simplicity.

The simplest reasonable assumption which can be made is that in a compressed sample wafer the pressure varies linearly with radial position. Such a relationship was found valid experimentally by Montgomery et al, although their evidence is not necessarily unambiguous. Following Montgomery et al, it will also be assumed that the pressure drops in a linear manner at the edge of the sample wafer to some small value comparable to the shear strength of the material. The pressure distribution can be represented analytically as

$$P(\rho) = P_c(1-\alpha\rho) \qquad 0 \leqslant \rho \leqslant \rho_e \tag{1a}$$

$$P(\rho) = P_c \left(\frac{1-\alpha\rho_e}{1-\rho_e}\right)(1-\rho) \qquad \rho_e \leqslant \rho \leqslant 1, \tag{1b}$$

where $\rho \equiv \frac{r}{a}$, that is, the radial position is expressed as a fraction of the anvil radius, a; Pc is the pressure at $\rho = 0$; and α is a constant which determines the pressure gradient. In writing Eq. (1b) it is assumed that the shear strength of the material is negligible compared to the pressures being applied, so that the pressure at $\rho = 1$ is taken to be zero. This is a reasonable approximation for use in the high-pressure realm of interest. The assumed pressure distribution is shown schematically in Figure 2.

If the nominal applied pressure is determined experimentally, as is generally the case, the central pressure, Pc, can be expressed as a function of α and ρ_e by integrating the pressure distribution over the anvil area and equating this quantity to the total applied force. Thus:

$$\bar{P} \equiv \frac{f}{\pi a^2} = \frac{1}{\pi} \int_0^1 P(\rho)\ 2\pi\rho\, d\rho\ . \tag{2}$$

Using Eq. (1) it is readily found that

$$P_c = f(\alpha, \rho_e)\, \bar{P} \tag{3a}$$

where

$$f(\alpha, \rho_e) = \frac{3}{1+(1-\alpha)\rho_e(1+\rho_e)}\ . \tag{3b}$$

Then Eq. (1) can be rewritten as

$$P(\rho) = f(\alpha, \rho_e)\, \bar{P}(1-\alpha\rho) \qquad 0 \leqslant \rho \leqslant \rho_e \tag{4a}$$

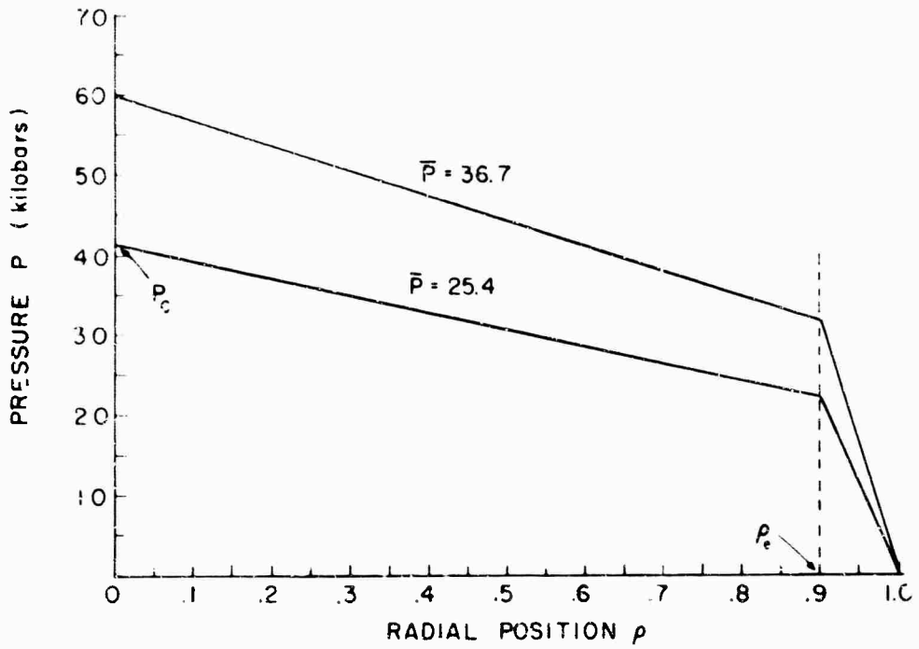

Figure 2. The Sample Pressure as a Function of Radial Position as Calculated from an Empirical Equation Derived in the Text

$$P(\rho) = g(\alpha, \rho_e)\, \bar{P}(1 - \rho) \qquad \rho_e \leqslant \rho \leqslant 1 \tag{4b}$$

where

$$g(\alpha, \rho_e) \equiv \left(\frac{1 - \alpha\rho_e}{1 - \rho_e}\right) f(\alpha, \rho_e)\,. \tag{5}$$

Although the experimental evidence is scant, an attempt will be made to determine the validity of the simple model being considered by comparing Eq. (4) with actual observations.

In experiments where calibrant wires are located at various radial positions Eq. (4) predicts a linear relationship between the ratio of transition pressure to nominal applied pressure and the radial position over the central portion of the anvils, that is,

$$\frac{P_t}{\bar{P}} = f(\alpha, \rho_e)\,(1 - \alpha\rho) \qquad \rho \lesssim \rho_e\,. \tag{6}$$

From Figure 1 it appears that the data obtained with the AFCRL press approximately meet this requirement. However, there is some indication that the reciprocal function $\overline{P}/P_t$ results in a better straight-line fit, which would have been predicted if the pressure distribution had been assumed to be given by

$$P(\rho) = P_c \frac{1}{1+\beta\rho} \qquad 0 \leqslant \rho \leqslant \rho_e \tag{7a}$$

$$P(\rho) = P_c \frac{(1-\rho)}{(1+\beta\rho_e)(1-\rho_e)} \qquad \rho_e \leqslant \rho \leqslant 1 . \tag{7b}$$

Using Eq. (7) and balancing forces, P_c can be eliminated as above. Thus

$$P(\rho) = \frac{\overline{P}}{h(\beta, \rho_e)(1+\beta\rho)} \qquad 0 \leqslant \rho \leqslant \rho_e \tag{8a}$$

$$P(\rho) = \frac{\overline{P}(1-\rho)}{i(\beta, \rho_e)} \qquad \rho_e \leqslant \rho \leqslant 1 \tag{8b}$$

where

$$h(\beta, \rho_e) \equiv \frac{2}{\beta^2}\left[\beta\rho_e - \ln(1+\beta\rho_e)\right] + \frac{1}{3}\left(\frac{1+\rho_e - 2\rho_e^2}{1+\beta\rho_e}\right) \tag{9}$$

and

$$i(\beta, \rho_e) \equiv h(\beta, \rho_e)(1+\beta\rho_e)(1-\rho_e) . \tag{10}$$

Then the equation analogous to Eq. (6) is:

$$\frac{\overline{P}}{P_t} = h(\beta, \rho_e)(1+\beta\rho) \qquad \rho \leqslant \rho_e . \tag{11}$$

Therefore over the central portion of the anvils the pressure distribution assumed in Eq. (7) results in a linear relationship between the ratio $\overline{P}/P_t$ and ρ as expressed in Eq. (11).

The data appear to fit Eq. (11) slightly better than Eq. (6), although the scatter and reproducibility of the data are such that a significant choice cannot be made between these alternative formulations. The measurements made by Myers et al were made at only a few values of ρ and show more scatter than the present results so that their data also do not permit a decisive choice. The measurements by Montgomery et al, however, are much more accurate. In their initial measurements using bismuth calibrant wires it was shown that the data fit an equation of the form of Eq. (11) very well. In the latter measurements using manganin wires it was shown that Eq. (6) was applicable. This contradiction is more apparent than real, however, because when β is small, Eq. (11) is equivalent to Eq. (6). Thus it is not possible with the experimental data available to make a clear choice between the alternative pressure distributions suggested. Clearly, more detailed data are needed. However there is no need at present to assume a more complex pressure distribution than those that have been considered. Accordingly, the linear pressure gradient given by Eq. (4) will be accepted tentatively as valid for the purpose of continuing calculations.

It should be noted that both of the pressure distributions suggested are slightly unrealistic in that they predict a cusp at the center of the anvils. Physically it is expected that $\frac{dP}{d\rho} = 0$ at this point. Most of the theoretical developments have also suffered from this difficulty, which, however, is not serious because only a very small fraction of the sample area at the center of the anvils is uncertain. It might be added that the pressure distribution given by Eq. (8) qualitatively resembles the theoretical predictions (Riecker and Seifert, 1964a).

The values of the constants α and ρ_e may be calculated from the slope and intercept of the straight line fitted to the data in Figure 1 according to Eq. (6). These values were found to be about 0.46 and 0.84 respectively, on the basis of a least-squares fit from which the uncertainties were estimated to be 10 percent and 5 percent, respectively. The radial pressure gradient existing in the sample wafer can be determined from Eq. (4). Thus

$$\frac{dP}{dr} = -\frac{f\alpha}{a}\,\bar{P} \qquad 0 \leqslant \rho \leqslant \rho_e \tag{12a}$$

and

$$\frac{dP}{dr} = -\frac{g}{a}\,\bar{P} \qquad \rho_e \leqslant \rho \leqslant 1. \tag{12b}$$

Over the central portion of the anvils, the pressure gradient in the AFCRL press is found to be $-3.4\bar{P}$ in the pressure range investigated. Thus at a nominal applied pressure of 30 kilobars a gradient of about 100 kilobars per inch would be present. The gradient in the annular ring around the periphery of the sample is much larger, amounting to about $-39\bar{P}$. These results may be compared with those of Montgomery et al, where the central gradient was found to be about $+0.47\bar{P}$ and the edge gradient amounted to about $-33\bar{P}$. The small central gradient they observed no doubt results from the Ag Cl composition of the central disc of the sample cell, which is a much more ductile material than the olivine used in the AFCRL tests. Similarly, the relatively close agreement on the edge gradient is probably connected with the fact that the pyrophyllite retaining rings used by Montgomery et al have mechanical properties more comparable to olivine. Montgomery et al also cited evidence which indicated that the pressure started dropping sharply about 0.030 in. in from the edge of the sample cell, that is, their results indicate $\rho_e = 0.88$ which is in reasonable agreement with the AFCRL measurements. In addition the compression tests on pyrophyllite wafers by Montgomery and Vaisnys indicated that an annular ring around the periphery of the sample supported only a small fraction of the applied load. For a wafer of the same initial thickness and diameter as those used in the AFCRL experiments their data indicate that 29.6 percent of the sample area was non-load-supporting, that is, ρ_e was about 0.84, in satisfactory agreement with the other observations made above.

These numerical comparisons indicate that the pressure distribution given by Eq. (4) is not seriously in error. This pressure distribution is shown in Figure 2, which uses the values of α and ρ_e deduced from the AFCRL data, assuming a nominal applied load of 25.4 or 36.7 kilobars. Note that a pressure multiplication effect of about 1.6 was observed.

The foregoing considerations lead to the conclusion that the existence of a large pressure multiplication effect, as indicated by data such as that shown in Figure 1, does not necessarily imply the existence of a large pressure gradient over the central portion of the sample cell. It may only mean that there is an annular region around the periphery of the sample which is not supporting its share of the applied load. This analysis and the available data do indicate that the magnitude of the pressure gradient over the central portion of the sample increases in proportion to the total applied load, and that the actual gradient present in a given situation will strongly depend on the composition and dimensions of the sample cell as well as on the total applied load. It is also clear that very large gradients are to be expected at the sample edge where a ring comprising as much as 30 percent of the total anvil area may be supporting only a small fraction of the applied load.

3.1 Static Anvil Experiments

The influence of a pressure distribution such as that given by Eq. (4) on various types of experiments will now be considered.

3.1.1 PHASE TRANSITIONS IN HOMOGENEOUS DISCS

First consider a case where the central portion of the sample wafer is a homogeneous material which undergoes a phase transition upon the application of high pressure. If α is positive, as is commonly the case, the pressure is greatest at the center of the sample wafer and the phase transition begins at the center when the nominal applied pressure reaches a value given by

$$\bar{P}_i = \frac{P_t}{f} , \tag{13}$$

where P_t is the true pressure at which the phase transition occurs.

As the pressure is increased the transformed region continues to increase in diameter until it extends over the entire area bounded by ρ_e. The nominal applied load then is given by

$$\bar{P}_f = \frac{P_t}{f(1 - \alpha\rho_e)} . \tag{14}$$

Further increasing the pressure will result in only a very slow increase in the area of the transformed material because of the very sharp pressure gradients existing near the edge of the sample cell. Thus the width of the phase transition, as reflected in the range of nominal applied pressures, required to drive it to completion can be determined from the difference of Eqs. (13) and (14). Thus

$$\Delta\bar{P} = \left(\frac{\alpha\rho_e}{1 - \alpha\rho_e}\right) \frac{P_t}{f} . \tag{15}$$

Note that this transition interval is due only to the pressure gradients; the actual transition is assumed to be perfectly sharp. In addition, the transition pressure determined by this hypothetical experiment can be determined by averaging Eqs. (13) and (14). Thus

$$\bar{P}_t = \left(\frac{2 - \alpha\rho_e}{1 - \alpha\rho_e}\right) \frac{P_t}{2f} , \tag{16}$$

where $\bar{P}_t$ is the transition pressure as determined in the hypothetical experiment.

Using the values of α, ρ_e, and f determined in the AFCRL experiments as illustrative of a typical case, it is found that

$$\bar{P}_i = 0.61\ P_t, \tag{17a}$$

$$\bar{P}_f = 0.99\ P_t, \tag{17b}$$

$$\Delta\bar{P} = 0.38\ P_t, \tag{17c}$$

$$\bar{P}_t = 0.80\ P_t. \tag{17d}$$

Thus the transition begins when the nominal applied pressure is only 61 percent of the true transition pressure and proceeds until it reaches 99 percent of the true pressure. The transition would appear sluggish, since the width would be about 38 percent of the transition pressure, and the average transition pressure deduced from this hypothetical experiment only, would be 80 percent of the true value.

Although this numerical example cannot be taken too seriously, it illustrates clearly the nature of the problems which can be encountered in the investigation of opposed anvils. The numerical values used to characterize the pressure distribution were shown previously to be generally compatible with those reported by other investigators. It is of interest to determine how these results would be affected by reasonable variations in the parameters α and ρ_e.

It is clear that if α is zero, the width of the transition will also be zero, but that the observed transition pressure will still be less than the true value because f has a value greater than 1.0 for any ρ_e less than 1.0. The detrimental effect of the non-load-bearing circumferential region is very evident. All of the experimental evidence available suggests that very little can be done experimentally to increase ρ_e above 0.9, although this factor depends somewhat on the sample material and dimensions. It is therefore clear that the nominal applied load, which is the quantity usually observed experimentally, may be considered a parameter which must be calibrated using known phase transitions as fixed points, or by some other means. When α is negative, as it was in the experiments of Montgomery et al, the error introduced by the negative pressure gradient over the central portion of the sample may compensate partially for the error introduced by the non-load-bearing peripheral region.

In a more common experimental arrangement the sample undergoing the phase transition is surrounded by a retaining ring of some other material. In this case, ρ_e should be replaced by ρ_r, that is, by a value indicative of the boundary between

the sample and the retaining ring. Inasmuch as ρ_r is usually less than ρ_e, the width of the transition would appear smaller, but the average transition pressure would be even more in error. In this modified example, the value of f is not changed as long as it is assumed that the pressure gradient remains the same.

Another factor which might affect the preceding analysis is the influence of any volume change associated with the phase transition. As the phase transition proceeds under increasing pressures the transformed material generally undergoes a reduction in volume, and hence it tends to withdraw support from the anvil. This causes an increase in the pressure applied to the low-pressure polymorph, and tends to drive the transformation to completion somewhat faster than was predicted by the simple model considered. Although the model could be made more sophisticated by considering volume effects, the numerical data available and the accuracy of the calculations that can be made do not justify the additional effort at present.

3.1.2 ELECTRICAL RESISTANCE DISCONTINUITIES

As a second example, consider the case in which a resistance element in the form of a wire or narrow ribbon is placed across the diameter of the anvil face. It is assumed that the wire is embedded in silver chloride or some other suitable pressure-transmitting medium, and that the pressure dependence of the resistance of the sample is observed. Consider in particular that the material undergoes a phase transition with which there is associated a discontinuity in electrical resistivity. This is the experimental arrangement commonly used by Bridgman and others.

The analysis given previously is directly applicable to this situation. It is highly unlikely that phase transitions could be located with precision from measurements of nominal applied pressure at which resistance discontinuities are observed. Thus it is not surprising that Bridgman's anvil measurements disagreed seriously with his piston and cylinder measurements where more nearly hydrostatic conditions prevailed. The pressure distribution in an anvil geometry approximating that used by Bridgman was measured by Montgomery et al and was discussed earlier. Montgomery et al found that the discrepancies in Bridgman's measurements could easily be accounted for by the observed pressure gradients.

3.2 Dynamic Anvil Experiments

The preceding discussion referred specifically to static anvils. When dynamic anvils are considered the problems become more complex. For example, the occurrence of a phase transition might be as described previously in some simple cases; however, shear strain frequently facilitates phase transitions and adds a complicating factor. In fact the effect of shear strain on reaction rate provides

the primary motivation for performing phase diagram studies and synthesis work on dynamic anvils.

An important application of dynamic anvils is the measurement of the shear strength of materials at high pressures. The AFCRL experiments have been discussed in detail elsewhere (Riecker and Seifert, 1964a, 1964b); however the essential features need to be described here briefly.

The sample consists of a homogeneous disc compressed between the anvils. One anvil is rotated at a constant rate by a suitable drive mechanism while the other is held stationary. The torque required to shear the sample is measured as a function of the applied load, temperature, and rate of strain. From these data and the known geometrical factors, the shear strength of the sample material may be determined as a function of pressure, temperature, and rate of strain.

Experimentally it is found that at low pressures the sample does not shear but rather that surface slippage occurs at the interface between the sample and anvil. As the pressure is increased, a point is reached at which the surficial friction stresses exceed the shear strength of the sample, and internal shearing begins. The pressure required to produce the transition from slippage to shearing varies greatly with the properties of the sample material; for the hard rock and mineral materials with which the authors are particularly concerned, shearing does not begin until pressures of about 30 kilobars are reached. A typical plot of turning moment, M, versus nominal applied pressure, P, is shown in Figure 3.

3.2.1 SURFICIAL FRICTION MEASUREMENTS

Consider first the low-pressure region in which surficial slippage occurs. Using the pressure distribution given by eq (4), and assuming the coefficient of friction between the sample material and anvil to be independent of pressure, the turning moment, M, can be found from

$$M = 2\pi a^3 \mu \int_0^1 P(\rho)\, \rho^2\, d\rho \tag{18a}$$

or

$$M = 2\pi a^3 \mu \int_0^{\rho_e} f(\alpha, \rho_e)\, \bar{P} \rho^2 (1 - \alpha\rho)\, d\rho$$

$$+ 2\pi a^3 \mu \int_{\rho_e}^1 g(\alpha, \rho_e)\, \bar{P} \rho^2 (1 - \rho)\, d\mu. \tag{18b}$$

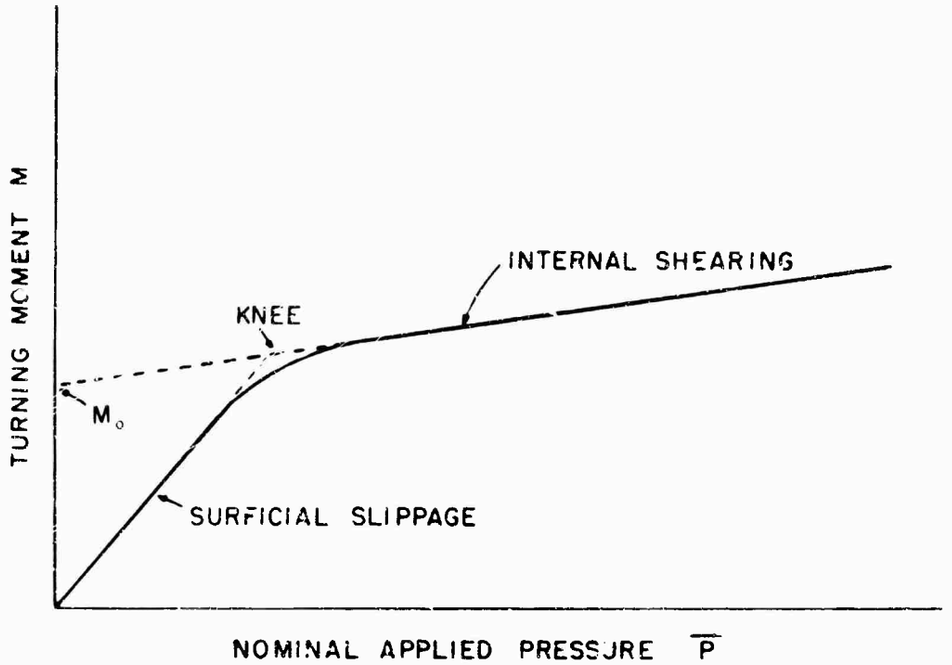

Figure 3. A Typical Plot of Turning Moment versus Nominal Applied Pressure as Observed in Shearing Experiments. The knee in the curve separates the low pressure realm in which surficial slippage occurs from the high pressure realm in which internal shearing of the sample occurs

This reduces to

$$M = \frac{2\pi a^3}{3} \mu \bar{P} \left\{ f\rho_e^3 \left(1 - \frac{3}{4}\alpha\rho_e\right) + g\left[\frac{1}{4} - \rho_e^3\left(1 - \frac{3}{4}\rho_e\right)\right] \right\}, \tag{19}$$

where the symbols have the same meanings used previously. Thus the friction coefficient can be calculated from

$$\mu = \frac{3Q(\alpha, \rho_e)}{2\pi a^3} \frac{M}{\bar{P}}, \tag{20}$$

where $Q(\alpha, \rho_e)$ is defined to be the reciprocal of the expression in brackets in Eq. (19).

Equation (20) is well established experimentally. Measurements made on mineral materials show the predicted linear increase in turning moment with pressure. In addition the numerical values for the friction coefficient agree with published data. Bridgman reported similar observations on a wide range of sample materials.

The quantity $Q(\alpha, \rho_e)$ is a correction factor which would be 1.0 in the ideal case of a completely uniform pressure, that is, when $\alpha = 0$ and $\rho_e = 1.0$. In any real experiment Q will deviate somewhat from unity, the extent of this deviation is the subject of interest. Numerical values of Q are shown graphically in Figure 4 for a range of values of α and ρ_e. Using the values of these parameters derived from the static AFCRL measurements, it is found that $Q \sim 1.10$, which means that friction coefficients calculated assuming $Q = 1.0$ will be too small by about 10 percent. However, this is a pessimistic estimate. The experimental observations discussed in Section 2 indicate that α is smaller and ρ_e larger under dynamic conditions. This probability is further supported by analysis of shear measurements given later. Thus it is reasonable to conclude that friction measurements made in this manner will not be in error by more than a few percent.

3.2.2 SHEAR STRENGTH MEASUREMENTS

In the high-pressure region surficial slippage ceases and the sample wafer experiences internal shearing. The shear strength of the material may be expected to be dependent on the pressure, temperature, and rate of strain in the general case. In order to analyze the problem several simplifying assumptions must be made. Thus it is assumed (1) that the shear strength of the material increases linearly with the applied pressure (2) that the temperature is uniform throughout the sample wafer, and (3) that the shear strength is independent of the rate of strain of the sample material.

The first assumption is generally compatible with the results obtained here and with numerous observations reported by Bridgman. It cannot be expected to hold in the vicinity of phase transitions, however. The second assumption is reasonable in view of the small thickness of the samples and the relatively high thermal conductivity and large mass of typical anvils. The third assumption is not generally valid. It was shown by Bridgman (1937) that the shear strength of some materials was independent of rate of strain if the experimental temperature was much lower than the melting point of the material. This condition is generally satisfied in the AFCRL experiments and only small rate effects have been observed over several orders of magnitude of anvil speed. The third assumption must be used with caution, however, because the rate of strain of the sample wafer varies from essentially zero at the axis of rotation to some large value at the periphery, depending on the rate of anvil rotation.

The transition from surficial slippage to internal shearing does not occur abruptly. Due to the pressure gradients present in the sample, a transition interval is encountered which results in the knee shown in Figure 3; the larger the gradients the wider the transition region.

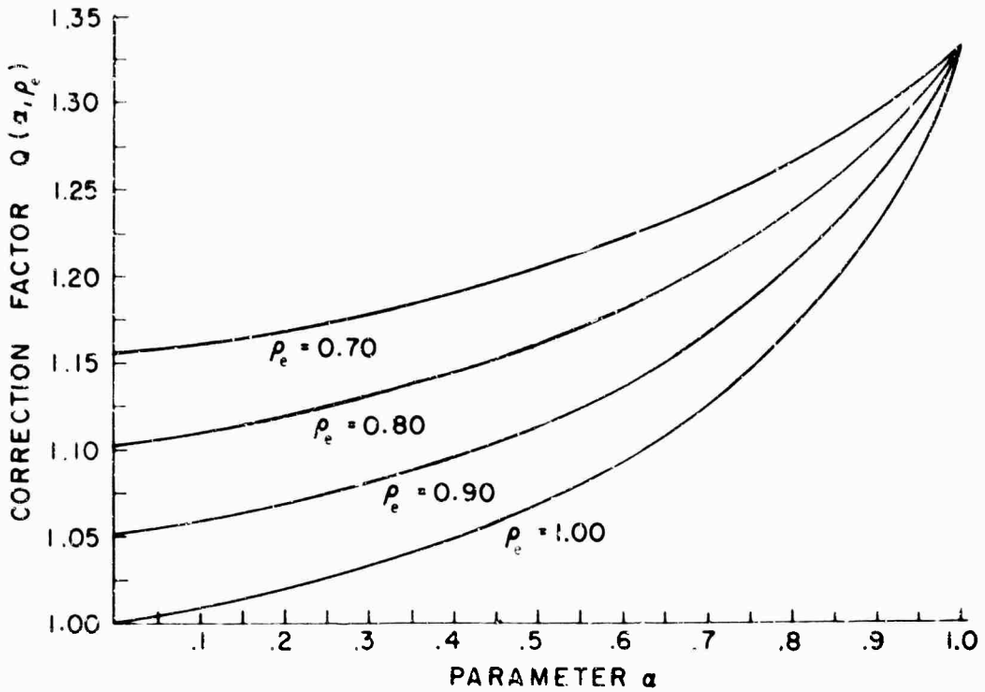

Figure 4. The Correction Factor $Q(\alpha, \rho_e)$ as a Function of the Parameters α and ρ_e. This factor is defined in the text, Eq. (20)

If it is assumed that the pressure distribution given by Eq. (4) is applicable, then the internal shearing will begin at the center of the sample when $\mu P_c = \tau$ where τ is the shear strength of the material. This is assumed to be linearly related to pressure as

$$\tau = S + \beta P, \tag{21}$$

where S is the shear strength of the material in the absence of hydrostatic pressure and β is a constant. S and β may be dependent on temperature but are assumed to be independent of rate of strain.

Under these conditions it is found that internal shearing will start at the center when the nominal applied pressure reaches the value

$$\bar{P}_i = \frac{S}{(\mu - \beta) f} . \tag{22}$$

As the pressure is increased the diameter of the sheared portion will increase rapidly until $\mu P(\rho_e) = \tau$, that is, until the radius of the sheared region reaches ρ_e.

Further increases in pressure will result in a more gradual increase in the shearing area because of the sharp drop in pressure near the sample edge. Thus the transition to shearing is nearly complete when

$$\overline{P}_f = \frac{S}{(\mu - \beta)(1 - \alpha\rho_e)f} \quad . \tag{23}$$

The width of the transition is readily found to be

$$\Delta\overline{P} = \frac{S}{(\mu - \beta)} \quad \frac{\alpha\rho_e}{(1 - \alpha\rho_e)f} \tag{24}$$

and the average pressure at which the transition occurs is given by

$$\overline{P}_N = \frac{S}{(\mu - \beta)f} \left(\frac{2 - \alpha\rho_e}{1 - \alpha\rho_e} \right) \quad . \tag{25}$$

Thus the ratio of these quantities is

$$\frac{\Delta\overline{P}}{\overline{P}_N} \equiv R(\alpha, \rho_e) = \frac{2\alpha\rho_e}{2 - \alpha\rho_e} \quad . \tag{26}$$

The ratio $R(\alpha, \rho_e)$ is shown in Figure 5 for an appropriate range of the parameters. Note that this ratio is dependent on the form of the pressure gradient, but is not explicitly dependent on the properties of the material being sheared. Equation (26) is also applicable to phase transformations provided the transformation is not influenced by shear or is observed under static conditions.

Numerical values of the ratio $R(\alpha, \rho_e)$ can be obtained from experimental data which will permit some limits to be placed on the pressure distribution under dynamic conditions. For example, the AFCRL measurements on minerals indicate that $\Delta\overline{P}$ is definitely less than 5 kilobars while $\overline{P}_N$ is about 30 kilobars. Thus R is less than 0.17 in these experiments. Reference to Figure 5 reveals that for ρ_e in the range 0.9 to 1.0, α is less than 0.17, that is, much less than observed in the static experiments on olivine. Thus the width and location of the knee in the plot of turning moment versus nominal applied pressure provides an internal check on the pressure gradients present in the shear experiments and corroborates the qualitative observations made earlier.

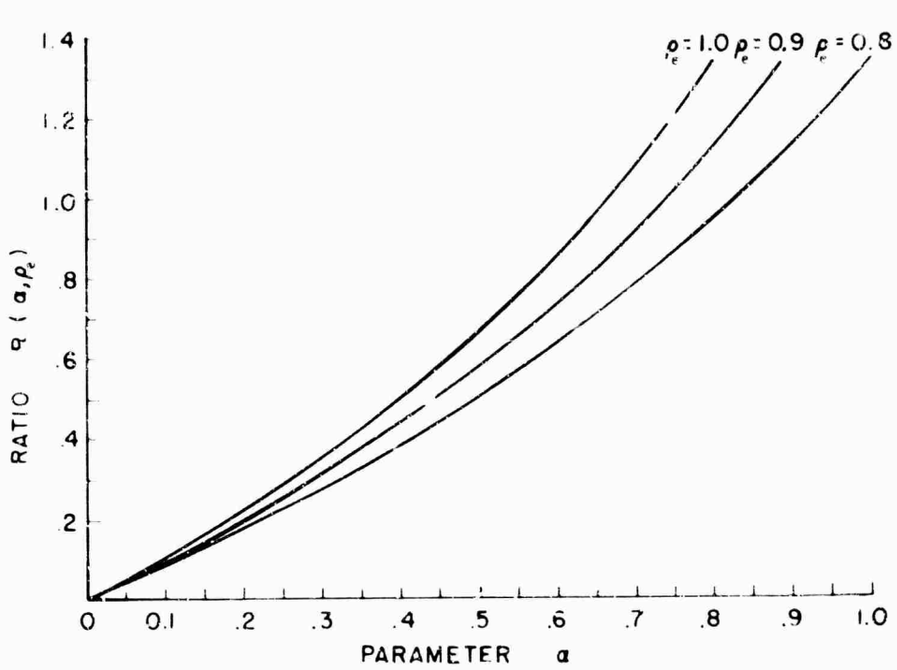

Figure 5. The ratio $R(\alpha, \rho_e)$ as a Function of the Parameters α and ρ_e. This factor is defined in the text, Eq. (26)

The turning moment required to shear the sample wafer may be computed from the integral

$$M = 2\pi a^3 \int_0^1 \tau (P) \rho^2 d\rho . \tag{27}$$

Considering the high-pressure realm where the radius of the shearing region is ρ_e or greater, and using the usual pressure distribution, this integral can be written as

$$\frac{M}{2\pi a^3} = \int_0^{\rho_e} \left[S + \beta f \bar{P} (1 - \alpha\rho) \right] \rho^2 d\rho$$

$$+ \int_{\rho_e}^{\rho_x} \left[S + \beta g \bar{P} (1 - \rho) \right] \rho^2 d\rho$$

$$+ \int_{\rho_x}^{1} \mu g \bar{P} (1 - \rho) \rho^2 d\rho \quad . \tag{28}$$

Here ρ_x is the radius marking the outer boundary of the shearing region. Although this general expression can be readily integrated, it is more convenient for numerical calculations to consider two special cases, that is, when $\rho_x = \rho_e$ and when $\rho_x = 1.0$. The former case corresponds to the most unfavorable situation which applies above the "knee" in the turning moment curve (Figure 3). In this case only surficial slip occurs in the annular region between $\rho = \rho_e$ and $\rho = 1.0$. The second case to be considered applies in the very-high-pressure realm where the material in the annular ring is also being sheared.

In the first case the turning moment is:

$$M = \frac{2\pi a^3}{3}\left[\rho_e{}^3 S + \overline{P}\left\{\beta\,\rho_e{}^3 f\left(1 - \frac{3}{4}\alpha\rho_e\right) + \mu g\left[\frac{1}{4} - \rho_e{}^3\left(1 - \frac{3}{4}\rho_e\right)\right]\right\}\right] \tag{29}$$

while in the latter case it takes the simpler form:

$$M = \frac{2\pi a^3}{3}\left[S + \beta\,\overline{P}\left\{\rho_e{}^3 f\left(1 - \frac{3}{4}\alpha\rho_e\right) + g\left[\frac{1}{4} - \rho_e{}^3\left(1 - \frac{3}{4}\rho_e\right)\right]\right\}\right]. \tag{30}$$

The linear relationship between M and $\overline{P}$ predicted by Eqs. (29) or (30) is in agreement with measurements made on mineral materials in the AFCRL apparatus as well as with many measurements made by Bridgman (1935, 1936, 1937). The constants S and β can be determined from the intercept and slope, respectively, of a plot of turning moment versus nominal applied pressure. When these graphically determined factors are inserted into Eq. (21) the pressure dependence of the shear strength of the material under test is found from the following two expressions corresponding to the two special cases under consideration:

$$\tau(P) = \frac{3}{2\pi a^3}\left\{\rho_e{}^{-3} M_0 + T(\alpha, \rho_e, \mu Z)\,\frac{dM}{d\overline{P}}\,P\right\} \tag{31}$$

or

$$\tau(P) = \frac{3}{2\pi a^3}\left\{M_0 + Q(\alpha, \rho_e)\,\frac{dM}{d\overline{P}}\,P\right\}. \tag{32}$$

In these expressions M_0 is the intercept found by extrapolation as indicated in Figure 3, $Q(\alpha, \rho_e)$ remains as previously defined, and $T(\alpha, \rho_e, \mu Z)$ is given by

$$T(\alpha, \rho_e, \mu Z) = \frac{1 - \mu Z g\left[\frac{1}{4} - \rho_e^3 \left(1 - \frac{3}{4}\rho_e\right)\right]}{\rho_e^3 \, f\left(1 - \frac{3}{4}\alpha\rho_e\right)}, \tag{33}$$

where

$$Z \equiv \frac{2\pi a^3}{3} \frac{d\bar{\sigma}}{dM} \quad . \tag{34}$$

Consider first the unfavorable case depicted by Eq. (31). Two correction factors, ρ_e^{-3} and T, are encountered which are normally assumed to be unity in the calculation of shear strengths. The neglect of these factors can lead to appreciable errors, depending on the pressure gradients present. For example, ρ_e^{-3} takes on the values 1.37, 1.17 and 1.00 when ρ_e assumes the values 0.90, 0.95, and 1.00, respectively. Thus the first term in Eq. (31) may be in error by as much as 37 percent under unfavorable conditions.

The function $T(\alpha, \rho_e, \mu Z)$ cannot be calculated in the general case because of the presence of the factor $Z\mu$, but for the mineral materials of particular interest this quantity is found to have the value 2.0. For this special case the function $T(\alpha, \rho_e, \mu Z)$ has been plotted in Figure 6 for an appropriate range of the parameters. Note that this quantity may be either greater or less than unity. For a reasonable range of parameters, such as $\rho_e > 0.9$ and $\alpha < 0.2$, it is clear that the second term in Eq. (31) should not be in error by more than 12 percent.

These considerations lead to the conclusion that shear strengths calculated from Eq. (31) with the assumption that ρ_e and T are unity will be too small by as much as 38 percent at very low pressures, and too large by at most 12 percent at very high pressures. At intermediate pressures the error will be somewhere between these extremes depending on the relative magnitude of the two terms on the right hand side of Eq. (31). It is also apparent that the error arises primarily from the fact that $\rho_e \neq 1$. Thus an annular ring of material around the periphery of a sample which is not sheared can be very detrimental.

Consider now the most favorable case which can occur, that is, when $\rho_x = 1.0$ and the entire sample is sheared. The shear strength is given by Eq. (32) and there is only one correction factor, $G(\alpha, \rho_e)$, which is plotted in Figure 4. For reasonable values of the parameters, that is, $\rho_e > 0.9$ and $\alpha < 0.2$, it is found that the error in the second term of Eq. (32) should be less than 7 percent. Thus the shear strengths calculated from Eq. (32) would be in error by a negligible amount at very low pressures while they would be too small by as much as 7 percent at very high pressures.

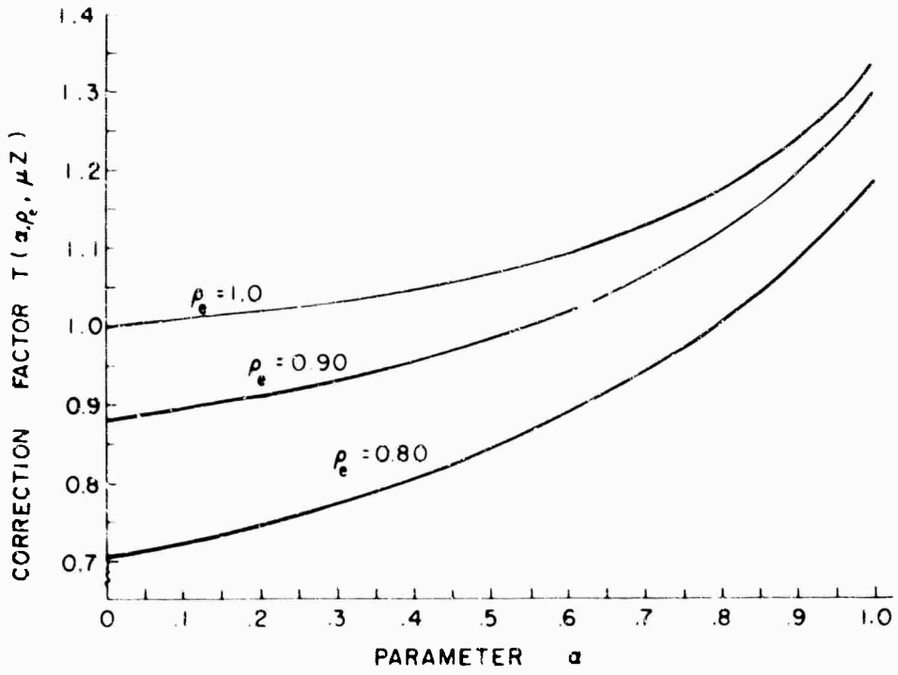

Figure 6. The Correction Factor $T(\alpha, \rho_e, \mu Z)$ as a Function of the Parameters α and ρ_e for the Special Case $\mu Z = 2.0$. These factors are defined in the text, Eqs. (33) and (34)

On the basis of these two limiting cases it is reasonable to conclude that shear strength measurements made in dynamic anvils will not be grossly in error, even in the presence of rather substantial pressure gradients. In the measurements on minerals just presented, it seems probable that the computed shear strengths are not in error by more than 10 percent. However, it is clear that the peripheral region around the edge of the sample disc where the pressure drops rapidly has a decisive bearing on the accuracy of these calculations as well as on those discussed previously. The width of this peripheral region as characterized by ρ_e remains a largely unknown but crucial factor, especially in dynamic anvils.

4. CONCLUSIONS

The experimental evidence relative to the pressure gradients in opposed anvil devices was reviewed briefly in Section 1 and some new observations were given in Section 2. The data were found to be generally consistent. A compressed sample may be divided conveniently into two major regions: (1) A central portion comprising about 75 percent of the anvil area, in which the pressure usually decreases

toward the sample edge, although a negative gradient may be present under some conditions, for example, when the sample cell has a very large diameter-to-thickness ratio. (2) An annular ring around the periphery of the sample comprising about 25 percent of the area, where the pressure drops rapidly to some small value indicative of the shear strength of the material.

Section 3 gave an empirical formula, assuming a linear gradient, for the pressure distribution in these two regions, which was found to be compatible with the experimental observations. This pressure distribution was used to estimate the errors which might be introduced into various types of anvil experiments by the pressure gradients. It was found that appreciable errors can arise, and correction factors were given graphically for a variety of conditions. Analysis of some shear experiments indicated that the pressure gradients are much smaller under dynamic conditions than under static conditions.

These considerations, although generalized, have shown that in anvil experiments very careful consideration must be given to the effects of pressure gradients. In static experiments the sample geometry may be adjusted and proper calibration procedures used such that only minor errors are introduced. Under dynamic conditions very little can be done to modify the pressure gradients and it is fortunate that the shearing of the sample cell tends to bring about a more uniform pressure distribution. The analysis presented has shown that in many instances the peripheral region, which is partially non-load-supporting, has a greater detrimental effect on anvil experiments than does the pressure gradient which exists over the central portion of the sample cell.

The empirical analysis in Section 3 provides some insight into the problems which can arise in anvil experiments due to the presence of pressure gradients, and, provided some knowledge of the pressure gradients is available, it permits rough computations of the errors. It is hoped that additional systematic investigations will be made into the nature and magnitudes of pressure gradients so that these ideas may be more rigorously applied or more sophisticated ones developed.

BLANK PAGE

Acknowledgments

The authors are grateful to Dr. N. A. Haskell for providing extensive technical assistance. The Advanced Projects Agency provided funds for fabrication of the shear press as part of VELA-UNIFORM under Contract AF19(628)-1646.

References

Bridgman, P. W. (1935) Effects of high shearing stress combined with high hydrostatic pressure, Phys. Rev. 48:825.

Bridgman, P. W. (1936) Shearing phenomena at high pressure of possible importance to geology, J. Geol. 44:653.

Bridgman, P. W. (1937) Shearing Phenomena at high pressures, particularly in inorganic compounds, Proc. Am. Acad. Arts Sci. 71:387.

Christiansen, E. B., et al (1962) Irreversible compressibility of silica glass as a means of determining the distribution of force in high pressure cells, Jour. Am. Cer. Soc. 45:172.

Duecker, H. C. and Lippincott, E. R., Distribution of Pressure in an Opposed-Anvil High-Pressure Cell, ASME Paper No. 64 WA/PT-15, to be published.

Jackson, J. W. and Waxman, M. (1962) An analysis of pressure and stress distribution under rigid bridgman-type anvils (in High Pressure Measurement, Giardini and Lloyd Ed), Butterworths, London.

Jackson, J. W. and Davis, R. L. An Analysis of the Stress Distribution under Elastically Deformable Bridgman-type Pressure Anvils, ASME Paper No. 64-WA/PT-27, to be published.

Jamieson, J. C. and Lawson, A. W. (1962) X-ray diffraction studies in the 100 kilobar pressure range, J. Appl. Phys. 33:776.

Myers, M. et al (1963) Contribution to calibration of high pressure systems from studies in an opposed anvil apparatus (in High Pressure Measurement. Giardini and Lloyd, Ed), Butterworths, London.

Montgomery, P. W. et al (1963) Calibration of Bridgman Anvils, A pressure scale to 125 kb (in High Pressure Measurement, Giardini and Lloyd, Ed), Butterworths, London.

Riecker, R. E. (1964) New shear apparatus for temperatures of 1000°C and pressures of 50 kb, Rev. Sci. Instr. 35:595.

Riecker, R. E. and Seifert, K. E. (1964a) Shear deformation of upper mantle mineral analogs: Tests to 50 kb at 27°C, Jour. Geophys. Res. 69:3901.

Riecker, R. E. and Seifert, K. E. (1964b) Olivine shear strength at high pressures and room temperature Bull. Geol. Soc. Amer. 75:571.

Vaisnys, R. J. and Montgomery, P. W. (1964) Materials for ultrahigh pressure sealing in Bridgman anvil devices, Rev. Sci. Instr. 35:985.

INSTRUMENTATION PAPERS
(Formerly: Instrumentation for Geophysics and Astrophysics)

No. 1. A Digital Electronic Data Recording System for Pulse-Time Telemetering, *Gilbert O. Hall, Feb 1953.*
No. 2. A Rocket-Borne Equipment for the Measurement of Infrared Radiation, *R. M. Slavin, Feb 1953.*
No. 3. Balloon-Borne Conductivity Meter, *S. C. Coroniti, A. Nazarek, C. S. Stergis, D. E. Kotas, D. W. Seymour and J. V. Werme, Dec 1954.*
No. 4. Magnetic Compensation of Aircraft, *J. McClay and B. Schuman, Aug 1955.*
No. 5. Lovotron-A Low Voltage Triggered Gap Switch, *E. H. Cullington, W. G. Chace and R. L. Morgan, Sep 1955.*
No. 6. Balloon-Borne Air Sampling Device, *Charles W. Chagnon, Apr 1957.*
No. 7. Instrumentation for Studies of the Exploding Wire Phenomena, *W. G. Chace and E. H. Cullington, Aug 1957.*
No. 8. Device for Lowering Loads from High-Altitude Balloons, *W. C. Wagner and F. X. Doherty, Jul 1958.*
No. 9. Equipment and Techniques for In-Flight Deployment of Long Train Instrumentation Packages from High Altitude Balloons, *Arlo E. Gilpatrick and Romain C. Fruge, Sep 1958.*
No. 10. Study of a Phosphor Light Pulser, *Michael R. Zatzick, Sep 1960.*
No. 11. Study of a Pulsed Logarithmic Photometer, *Michael R. Zatzick, Sep 1960.*
No. 12. Theoretical Analysis of the PAR-Scope: An Oscilloscope Display for Weather Radars, *Edwin Kessler, III, Jul 1959.*
No. 13. Evaluation of Visual Distance Computer, CP-384(XD-1), *P. I. Hershberg, Apr 1960.*
No. 14. Hypsometer for Constant Level Balloon, *W. C. Wagner, Jun 1960.*
No. 15. Magnetic Photomultiplier with Large Cathode for Extreme Ultraviolet, *L. A. Hall and H. E. Hinteregger, Dec 1960.*
No. 16. AIDE – Altitude Integrating Device, Electronic, *P. I. Hershberg, J. R. Griffin and R. H. Guenthner, Dec 1960.*
No. 17. Switching Devices for Very High Currents, *E. H. Cullington and W. G. Chace, April 1961.*
No. 18. Cedar Hill Meteorological Research Facility, *D. W. Stevens, Jun 1961.*
No. 19. Evaluation of Control Monitor AN/GGA 11 Prototype, *R. S. Menchel, Aug 1961.*
No. 20. A Microwave Refractometer with Fast Reaponse and Absolute Digital Recording, *R. H. Shaw and R. M. Cunningham, Mar 1962.*
No. 21. Superpressure Balloon for Constant Level Flight, *L. Gruss, Jul 1962.*
No. 22. Measurement Range Required of Meteorological Equipment, *A. Court and H. Salmela, Aug 1962.*
No. 23. Proportional Counter Spectrometer for Solar X-Rays Between 1 and 10 Angstroms, *J. Heroux, J. E. Manson, and R. Smith, Dec 1962.*
No. 24. A Simplified Sonic Anemometer for Measuring the Vertical Component of Wind Velocity, *J. Chandran Kaimal, Jan 63.*
No. 25. Evaluation of Modification to Antenna of Rawin Set AN/GMD-2, *Konstantin Pocs, Jan 63.*
No. 26. Evolution of the Design of the Anna I Satellite Optical Beacon, *T. Wirtanen, Feb 63.*
No. 27. Seismic Model Impactor, *K. C. Thomson and J. A. Hill, Aug 63.*
No. 28. Error Analysis of the Modified Humidity-Temperature Measuring Set AN/TMQ-11, *R. W. Lenhard, Jr., Major, USAF, and B. D. Weiss, Aug 63.*
No. 29. Evaluation of a Varacter Diode Parametric Amplifier for Rawin Set AN/GMD-2, *Konstantin Pocs, Sep 1963.*
No. 30. The Hydromagnetic Wave Tube, *R. E. Murphy and M. H. Bruce, Sep 1963.*
No. 31. A Time-of-Flight Mass Spectrometer Adapted for Studying Charge Transfer, Ion Disaociation, and Photoionization, *W. Hunt, Jr., et al., Sep 1963.*
No. 32. Moire Fringe Measuring System for Far Infrared Interferometric Spectrometer, *E. V. Loewenstein, Sep 1963.*
No. 33. Opposed Anvil Basic Design Considerations, *R. E. Riecker, 1/Lt USAF, Dec 1963.*
No. 34. New Shear Apparatus for Temperatures of 1000°C and Pressures of 50 kb, *R. E. Riecker, 1/Lt USAF, K. E. Seifert, 1/Lt USAF, Nov 1963.*
No. 35. Accuracy of Meteorological Data Obtained by Tracking the ROBIN With MPS-19 Radar, *Robert W. Lenhard, Jr., Major, USAF, Margaret P Doody, Dec 1963.*
No. 36. An Application of Induction Heating to Rock Deformation Apparatus, *R. E. Riecker, 1/Lt, USAF, Mar 1964.*
No. 37. A Monopole Phased-Array Feed for Spherical Reflectors, *W. G. Mavroides, L. S. Dorr, April 1964.*
No. 38. Equipment and Techniques for Low Temperature Electron Irradiations, *L.F. Lowe, C. Jimenez, and E.A. Burke, April 1964 (REPRINT).*
No. 39. Lunar Thermal Emission Measurements and Related Antenna Considerations, *John P. Castelli, April 1964 (REPRINT).*
No. 40. Continuous Zone-Refining Apparatus, *John K. Kennedy, April 1964 (REPRINT).*

INSTRUMENTATION PAPERS (Continued)

No. 41. Improved Closed-System Evaporation Crystallizer, *John L. Sampson and Mary A. DiPietro, May 1964 (REPRINT).*

No. 42. Calibration of a Flyable Mass Spectrometer for N and O Atom Sensitivity, *R.S. Narcisi, H.I. Schiff, J.E. Morgan and H.A. Cohen, June 1964 (REPRINT).*

No. 43. A Preliminary Evaluation of the Cricketsonde Rocket System, *Konstantins Pocs, June 1964.*

No. 44. New Shear Apparatus for Temperatures of 1000°C and Pressures of 50 Kilobars, *R.E. Riecker, August 1964 (REPRINT).*

No. 45. Reflection Correction for Thermal Neutron Spectra Derived from Transmission Data, *E.A. Burke and L.F. Lowe, August 1964 (REPRINT).*

No. 46. A Prototype Lunar Transponder, *Wahlon S. Hunt, August 1964 (REPRINT).*

No. 47. Automatic Plotting of Spin-Wave Instability Threshold Data, *Tom G. Purnhagen, Capt, USAF, August 1964 (REPRINT).*

No. 48. Logical Techniques for Glottal Source Measurements, *John L. Ramsey, 1/Lt, USAF, August 1964.*

No. 49. An Ultrastable Microwave Radiometer, *William B. Goggins, Jr., Capt, USAF, September 1964.*

No. 50. Impurities in a Vacuum, *Jerome H. Bloom, Charlotte E. Ludington, and Robert L. Phipps, May 1964.*

No. 51. Digital Readout of Oscilloscope Sweep Delay Times, *K.E. McGee and W.W. Hunt, Jr., October 1964 (REPRINT).*

No. 52. High Pressure Thrust Bearings: An Application, *R.E. Riecker and D.L. Pendleton, November 1964.*

No. 53. A Method for Electrocutting Single Crystals of Metals and Electropolishing the Exposed Crystalline Face, *Bernard Rubin and John J. O'Connor, December 1964.*

No. 54. Comparison of Bivane and Sonic Techniques for Measuring the Vertical Wind Component. *J.C. Kaimal, H.E. Cramer, F.A. Record, J.E. Tillman, J.A. Businger, and M. Miyake, December 1964 (REPRINT).*

No. 55. Experiences with the Impedance Probe on Satellites, *O.C. Haycock, K.D. Baker and J.C. Ulwick, January 1965 (REPRINT).*

No. 56. Silicon Current Amplifier for Microampere Current Levels, *b. Buchanan, S. Roosild, and R. Dolan, February 1965 (REPRINT).*

No. 57. A Multi-Level Radar Storm Contour Mapper. *William E. Lamkin and David Atlas, April 1965.*

No. 58. Nanosecond Pulses of Very Low Impedance, *Heinz J. Fischer, April 1965.*

No. 59. An Operational Amplifier Circuit for Characterization of Negative-Conductance Devices, *Virgil E. Vickers, April 1965 (REPRINT).*

No. 60. Multiband Spectral System for Reconnaissance, *Carlton E. Molineux, April 1965 (REPRINT).*

No. 61. Operating Characteristics of a Commercial Resistance-Strip Magnetic Electron Multiplier, *W.W. Hunt, Jr., K.E. McGee, and M.J. Kennedy, May 1965 (REPRINT).*

No. 62. Frequency Stability in Dielectric Resonators, *M.R. Stiglitz and J.C. Sethares, May 1965 (REPRINT).*

No. 63. ANNA Satellite Yields Photogrammetric Parameters, *Owen W. Williams, June 1965 (REPRINT).*

No. 64. Heat Transfer Considerations in the Temperature Control of Instrumentation Packages at High Altitudes, *Arnold Piacentini, Kenneth H. Lindenfelser, 1/Lt, USAF, and Darrel E. Dube, 1/Lt, USAF, June 1965.*

No. 65. Vacuum Ultraviolet Light Sources: New Excitation Unit for the Rare Gas Continua, *R.E. Huffman, J.C. Larrabee, and Derek Chambers, June 1965.*

No. 66. The Compensation of Two-Beam Interferometers, *W.H. Steel, June 1965.*

No. 67. A Laser Fog Disdrometer, *Bernard A. Silverman, Brian J. Thompson, and John H. Ward, June 1965 (REPRINT).*

No. 68. Radiochemical Procedures for Selected Radionuclides in Environmental Samples, *Joseph Pecci, Peter J. Drevinsky, Edward Couble, Noreen A. Dimond, Marvin I. Kalkstein, and Anahid Thomasian, June 1965.*

No. 69. Evaluation of the T-755/GMQ-20 Wind Speed and Direction Transmitter, *Russell M. Peirce, Jr., June 1965.*

No. 70. A Laser for an Earth-Based Satellite Illuminator, *Robert L. Iliff, June 1965.*

No. 71. A Unique Scintillation Rate Counter for Ionospheric Studies, *Frederick F. Slack and John P. Mullen, June 1965.*

No. 72. Differential Thermal Analysis (DTA) of Oxide Systems in Air to 1620°C at Atmospheric Pressure, *Cortland O. Dugger, June 1965.*

No. 73. Automatic Camera System for Solar Corona Photography, *D.J. Davis, Jr., W.R. McCann, V.A. Remillard, P. Beaudoin, and A. Thomas, July 1965 (REPRINT).*

No. 74. A Direct Calibration of a Birefringent Photometer, *G.J. Hernandez and E.L. Layman, August 1965 (REPRINT).*

No. 75. A Ray-Tracing Program for Birefringent Filters, *J.M. Beckers, and R.B. Dunn, August 1965.*

INSTRUMENTATION PAPERS (Continued)

No. 76. Vocal-Response Synthesizer, *Caldwell P. Smith, August 1965 (REPRINT).*
No. 77. The Backfire Antenna: New Results, *Hermann W. Ehrenspeck, September 1965 (REPRINT).*
No. 78. A Method for Accurately Measuring the Vertical Electric Field Strength of a Propagating VLF Wave, *R.P. Harrison and E.A. Lewis, September 1965 (REPRINT).*
No. 79. A System for the Determination of the Vertical Wind Profile From an Aircraft, *James F. Morrissey, September 1965.*
No. 80. A Parapropagation Pattern Classifier, *Herbert A. Glucksman, September 1965 (REPRINT).*
No. 81. Pressure Gradients in Bridgman Anvil Devices, *L.C. Towle and R.E. Riecker, September 1965.*

DOCUMENT CONTROL DATA - R&D

(Security classification of title, body of abstract and indexing annotation must be entered when the overall report is classified)

1. ORIGINATING ACTIVITY *(Corporate author)*
Hq AFCRL, OAR (CRJ)
United States Air Force
Bedford, Massachusetts

2a. REPORT SECURITY CLASSIFICATION
Unclassified

2b. GROUP
-

3. REPORT TITLE

Pressure Gradients in Bridgman Anvil Devices

4. DESCRIPTIVE NOTES *(Type of report and inclusive dates)*
Scientific Report. Interim

5. AUTHOR(S) *(Last name, first name, initial)*

TOWLE, L.C., and RIECKER, R.E.

6. REPORT DATE
September 1965

7a. TOTAL NO. OF PAGES
40

7b. NO. OF REFS
14

8a. CONTRACT OR GRANT NO. Contract AF 19(628)-1646 Vela Uniform

b. PROJECT AND TASK NO. 7639-05

c. DOD ELEMENT 62405394

d. DOD SUBELEMENT 681000

9a. ORIGINATOR'S REPORT NUMBER(S)
AFCRL-65-707

9b. OTHER REPORT NO(S) *(Any other numbers that may be assigned this report)*
AFCRL-65-707

10. AVAILABILITY/LIMITATION NOTICES Qualified requestors may obtain copies of this report from DDC. Other persons or organizations should apply to the Clearinghouse for Federal Scientific and Technical Information (CFSTI), Sills Building, 5285 Port Royal Road, Springfield, Virginia 22151.

11. SUPPLEMENTARY NOTES

12. SPONSORING MILITARY ACTIVITY
Hq AFCRL, OAR (CRJ)
United States Air Force
Bedford, Massachusetts

13. ABSTRACT

Experimental evidence regarding pressure gradients in Bridgman anvil devices is reviewed and some new experimental data are presented. Although there are many differences in details, all the experimental evidence is found to fit a general pattern. A simple empirical relationship describing the pressure distribution is derived which is consistent with experimental observation. The experimentally determined pressure is used to estimate errors introduced into various types of anvil experiments by pressure gradients. Numerical values for the correction factors are given in graphical form for a wide range of experimental conditions. Analysis of shear experiments indicates that pressure gradients are much smaller under dynamic conditions. Analysis also shows that the peripheral sample region which is partially non-load-supporting frequently has a greater detrimental effect on anvil experiments than does the pressure gradient which exists over the central portion of the sample cell.

DD FORM 1 JAN 64 1473

14. KEY WORDS	LINK A		LINK B		LINK C	
	ROLE	WT	ROLE	WT	ROLE	WT
Geophysics Shear strength Racks Seismology Pressure						

INSTRUCTIONS

1. ORIGINATING ACTIVITY: Enter the name and address of the contractor, subcontractor, grantee, Department of Defense activity or other organization *(corporate author)* issuing the report.

2a. REPORT SECURITY CLASSIFICATION: Enter the overall security classification of the report. Indicate whether "Restricted Data" is included. Marking is to be in accordance with appropriate security regulations.

2b. GROUP: Automatic downgrading is specified in DoD Directive 5200.10 and Armed Forces Industrial Manual. Enter the group number. Also, when applicable, show that optional markings have been used for Group 3 and Group 4 as authorized.

3. REPORT TITLE: Enter the complete report title in all capital letters. Titles in all cases should be unclassified. If a meaningful title cannot be selected without classification, show title classification in all capitals in parenthesis immediately following the title.

4. DESCRIPTIVE NOTES: If appropriate, enter the type of report, e.g., interim, progress, summary, annual, or final. Give the inclusive dates when a specific reporting period is covered.

5. AUTHOR(S): Enter the name(s) of author(s) as shown on or in the report. Enter last name, first name, middle initial. If military, show rank and branch of service. The name of the principal author is an absolute minimum requirement.

6. REPORT DATE: Enter the date of the report as day, month, year, or month, year. If more than one date appears on the report, use date of publication.

7a. TOTAL NUMBER OF PAGES: The total page count should follow normal pagination procedures, i.e., enter the number of pages containing information.

7b. NUMBER OF REFERENCES: Enter the total number of references cited in the report.

8a. CONTRACT OR GRANT NUMBER: If appropriate, enter the applicable number of the contract or grant under which the report was written.

8b, 8c, & 8d. PROJECT NUMBER: Enter the appropriate military department identification, such as project number, subproject number, system numbers, task number, etc.

9a. ORIGINATOR'S REPORT NUMBER(S): Enter the official report number by which the document will be identified and controlled by the originating activity. This number must be unique to this report.

9b. OTHER REPORT NUMBER(S): If the report has been assigned any other report numbers *(either by the originator or by the sponsor)*, also enter this number(s).

10. AVAILABILITY/LIMITATION NOTICES: Enter any limitations on further dissemination of the report, other than those imposed by security classification, using standard statements such as:

(1) "Qualified requesters may obtain copies of this report from DDC."

(2) "Foreign announcement and dissemination of this report by DDC is not authorized."

(3) "U. S. Government agencies may obtain copies of this report directly from DDC. Other qualified DDC users shall request through

_____."

(4) "U. S. military agencies may obtain copies of this report directly from DDC. Other qualified users shall request through

_____."

(5) "All distribution of this report is controlled. Qualified DDC users shall request through

_____."

If the report has been furnished to the Office of Technical Services, Department of Commerce, for sale to the public, indicate this fact and enter the price, if known.

11. SUPPLEMENTARY NOTES: Use for additional explanatory notes.

12. SPONSORING MILITARY ACTIVITY: Enter the name of the departmental project office or laboratory sponsoring *(paying for)* the research and development. Include address.

13. ABSTRACT: Enter an abstract giving a brief and factual summary of the document indicative of the report, even though it may also appear elsewhere in the body of the technical report. If additional space is required, a continuation sheet shall be attached.

It is highly desirable that the abstract of classified reports be unclassified. Each paragraph of the abstract shall end with an indication of the military security classification of the information in the paragraph, represented as *(TS), (S), (C), or (U).*

There is no limitation on the length of the abstract. However, the suggested length is from 150 to 225 words.

14. KEY WORDS: Key words are technically meaningful terms or short phrases that characterize a report and may be used as index entries for cataloging the report. Key words must be selected so that no security classification is required. Identifiers, such as equipment model designation, trade name, military project code name, geographic location, may be used as key words but will be followed by an indication of technical context. The assignment of links, rules, and weights is optional.